Separating real and apparent effects of cloud, humidity, and dynamics on aerosol optical thickness near cloud edges

Myeong-Jae Jeong[1,2] and Zhanqing Li[3,4]

Received 13 November 2009; revised 21 September 2010; accepted 23 September 2010; published 16 December 2010.

[1] Aerosol optical thickness (AOT) is one of aerosol parameters that can be measured on a routine basis with reasonable accuracy from Sun-photometric observations at the surface. However, AOT-derived near clouds is fraught with various real effects and artifacts, posing a big challenge for studying aerosol and cloud interactions. Recently, several studies have reported correlations between AOT and cloud cover, pointing to potential cloud contamination and the aerosol humidification effect; however, not many quantitative assessments have been made. In this study, various potential causes of apparent correlations are investigated in order to separate the real effects from the artifacts, using well-maintained observations from the Aerosol Robotic Network, Total Sky Imager, airborne nephelometer, etc., over the Southern Great Plains site operated by the U.S. Department of Energy's Atmospheric Radiation Measurement Program. It was found that aerosol humidification effects can explain about one fourth of the correlation between the cloud cover and AOT. New particle genesis, cloud-processed particles, atmospheric dynamics, and aerosol indirect effects are likely to be contributing to as much as the remaining three fourth of the relationship between cloud cover and AOT.

Citation: Jeong, M.-J., and Z. Li (2010), Separating real and apparent effects of cloud, humidity, and dynamics on aerosol optical thickness near cloud edges, *J. Geophys. Res.*, *115*, D00K32, doi:10.1029/2009JD013547.

1. Introduction

[2] Uncertainty related to aerosols, especially their interactions with clouds is one of the large sources of uncertainty in the current projections of climate change [*Intergovernmental Panel on Climate Change*, 2007]. To understand aerosol-cloud interactions and to pinpoint the associated uncertainties, accurate aerosol measurements made near various cloud systems under diverse dynamical and physical conditions over different regions are necessary [e.g., *Yuan et al.*, 2008]. Recently, several studies using satellite-based aerosol products reported correlations between aerosol optical thickness (AOT) and cloud amount (or spatial variability of cloud fraction) over many regions in the world [e.g., *Ignatov and Nalli*, 2002; *Jeong and Li*, 2005; *Kaufman et al.*, 2005; *Matheson et al.*, 2006; *Loeb and Schuster*, 2008]. While it is tempting to construe such findings as evidence of aerosol-cloud interactions, caution should be exercised as coincidence or artifact might be at play [*Yuan et al.*, 2008; *Loeb and Schuster*, 2008]. In fact, satellite aerosol retrievals near clouds are not reliable, which reduces a considerable amount of useful data, making it difficult to deduce value-added information on aerosols [e.g., *Jeong and Hsu*, 2008; *Hansell et al.*, 2009]. For instance, contamination due to subpixel and/or thin cirrus clouds has been suspected to be one of the major sources of uncertainties in the satellite-based AOT data, which could potentially result in an artificial relationship between aerosols and clouds [e.g., *Ignatov and Nalli*, 2002; *Jeong et al*, 2005; *Kaufman et al.*, 2005; *Zhang et al.*, 2005]. Also, it has been shown that enhanced multiple scattering of light in the vicinity of clouds can result in AOT overestimations from satellites [*Wen et al.*, 2007; *Marshak et al.*, 2008]. In this regard, clouds are regarded as a source of artifacts.

[3] However, some other studies indicated that clouds can have a real impact on AOT. For example, increased new particle genesis and cloud processed particles near clouds have been reported [*Hegg et al.*, 1990; *Hoppel et al.*, 1994; *Alkezweeny*, 1995; *Hegg et al.*, 2004]. In addition, it has also been argued that an increased cloud fraction accompanied by enhanced relative humidity (RH) can affect aerosols through the aerosol humidification effect (AHE; also known as aerosol swelling effect), resulting in correlation between cloud faction and AOT [e.g., *Ignatov and Nalli*, 2002; *Jeong and Li*, 2005; *Kaufman et al.*, 2005].

[4] While some studies reported the effects or artifacts of individual factors influencing AOT with detailed discussions (e.g., effects of humidity by *Öström and Noone* [2000], *Jeong et al.* [2007], *Koren et al.* [2007], *Su et al.* [2008], and *Twohy et al.* [2009]; effects of increased aerosol particle size near clouds by *Tackett and Di Girolamo* [2009]; artifacts of cloud

[1]Goddard Earth Sciences and Technology Center, University of Maryland Baltimore County, Baltimore, Maryland, USA.
[2]NASA Goddard Space Flight Center, Greenbelt, Maryland, USA.
[3]Department of Atmospheric and Oceanic Science and ESSIC, University of Maryland, College Park, Maryland, USA.
[4]School of Atmospheric Physics, Nanjing University of Information Science and Technology, Jiangsu, China.

0148-0227/10/2009JD013547

contamination by *Zhang et al.* [2005]; artifacts due to enhanced scattering near clouds by *Wen et al.* [2007]), few investigations were made to comprehensively understand and quantify the factors causing such correlation between cloud amount and AOT. Using satellite-based aerosol data, it would be very difficult to deal with the issue due to the assumptions made in aerosol retrievals and numerous factors affecting the accuracy of retrieval [e.g., *Jeong et al.*, 2005].

[5] On the other hand, ground-based measurements of AOT from Cimel Sun photometers operated under the protocols of the Aerosol Robotic Network (AERONET) [*Holben et al.*, 1998] are highly accurate with little, if any, contamination by clouds, even when the observations are made under partly cloudy conditions. One may thus use them together with measurements of clouds and meteorological parameters to investigate the relation between AOT and cloud. The ample measurements available from the U.S. Department of Energy's Atmospheric Radiation Measurement (ARM) program over the Southern Great Plains (SGP) site allow us to unravel this complex issue.

[6] In this study, we first report that the AOT from ground-based measurements is correlated with cloud cover (or fraction) for small and moderate aerosol loading (i.e., AOT < 1.0). Then, possible causes, including real effects and artifacts, are discussed, and the most likely scenarios are proposed. Thus, this study attempts to (1) evaluate various effects on the AOT from ground-based sensors and (2) separate the artifact from the real effect on the observed AOT. The results of this study will be useful to create "clean" aerosol products for the study of direct and indirect aerosol effects.

2. Data

[7] Aerosol measurements taken over the Southern Great Plains (SGP) Cloud And Radiation Testbed (CART) site (36.6°N, 97.5°W) under the aegis of the Department of Energy's (DOE) Atmospheric Radiation Measurement (ARM) program characterize the temporal variability, vertical distribution, and optical properties of aerosols in the region using a large array of state-of-the-art instruments. They include the Cimel Sun photometer, Multifilter Rotating Shadow Band Radiometer (MFRSR), Raman lidar, In Situ Aerosol Profiles (IAP) flights, and the Aerosol Observing System (AOS). The spatial variability of aerosols relies on a network of MFRSRs at the Central Facility (CF) and Extended Facilities (EF), together with satellite remote sensing.

[8] The major data employed for this study are AERONET Level 2.0 (cloud-screened and quality-assured) aerosol products derived from the Cimel Sun photometer at the Central Facility "Cart Site" for 2 years (2003–2004). AOT at 550 nm, which is a common wavelength for many applications, was derived via interpolation using AOT at 500 and 675 nm. The profiles for aerosol extinction and relative humidity (RH) from the Raman lidar [*Goldsmith et al.*, 1998; *Turner and Goldsmith*, 1999] are utilized to compute the aerosol extinction weighted column mean RH (see section 4.2 for details). Also employed are cloud cover and cloud mask data from the Total Sky Imager (TSI), which continuously monitored the sky conditions over the ARM SGP site (Central Facility). Details on the respective instruments are provided below.

2.1. AERONET Sun Photometer Measurements of AOT

[9] The AOT measured from the AERONET Cimel Sun photometers [*Holben et al.*, 1998] has been used in numerous studies concerning aerosols and their radiative and climatic effects. The Cimel Sun photometer has eight channels spanning the ultraviolet, visible, and near infrared (340, 380, 440, 500, 675, 870, 940, and 1020 nm). It is composed of two collimators: one for direct Sun measurements and the other for sky radiance measurements. Both collimators have an equal field of view (1.2°), but the aperture for the sky photometers is 10 times larger than that for the Sun photometer so that the necessary dynamic range to observe the sky is provided. One set of direct normal measurements is made every 15 min and one set of sky radiance measurements is made per hour. The AOT is calculated from the transmission obtained from direct normal measurements using the Beer-Bouguer-Lambert's law after accounting for the attenuation due to molecular scattering and trace gas absorption. The AOT is derived to an accuracy of ±0.02–0.04 at a relative optical air mass of 2 [e.g., *Eck et al.*, 1999; *Rainwater and Gregory*, 2005; *Eck et al.*, 2005].

[10] The primary issue that could interfere with the accuracy of the AERONET AOT is cloud screening. Therefore, a strict cloud-screening algorithm was developed [*Smirnov et al.*, 2000], which is based on a stability check on the triplet (i.e., three instantaneous and consecutive measurements at 30 s apart) that constitutes an observation (made every 15 min), a test of consistency in the values of AOT and Angstrom exponent with their diurnal variability. While the algorithm works effectively to get rid of most, if not all, cloud-contaminated data, it can be too strict to discard some variable aerosols like smoke plumes [*Kaufman et al.*, 2005]. Also, it may fail to detect very thin stable cirrus [*Kinne et al.*, 1997; *Kaufman et al.*, 2005]. For the SGP CART site, AERONET AOT measurements have been collected since 1994. We used 2 years (2003–2004) of level 2.0 (cloud-screened and quality-assured) AOT data for this study.

2.2. Cloud Cover From the Total Sky Imager

[11] The Total Sky Imager (TSI; Model 880) captures images of the sky during daytime using a charged-coupled device (CCD) imager looking down a mirror that reflects the hemispheric sky. A shadowband on the mirror blocks the direct sunlight in order to protect the optics of the imager and to provide a good sensitivity to both dark (blue sky) and bright (cloud) targets. The images are recorded as 24-bit color JPEG files at 352 × 288 pixel resolution. Fractional cloud cover is determined by examining the relationships between the colors of the acquired image pixels within the field of view of 160° (zenith angle less than 80°) to determine whether a pixel represents clear sky, thin, or opaque cloud [*Long et al.*, 2001]. The color relationship is based on the fact that molecular scattering is much stronger in the blue spectral range than in the red spectral range while clouds more or less equally scatter from blue to red spectral ranges. Although the solar disk is blocked, it is difficult to discriminate clear sky from clouds in the vicinity of the Sun and for the angular area centered on the solar azimuth angle (outlined by a green circle around the Sun in Figure 1). This is because the intensity range of the CCD camera is limited compared to the very

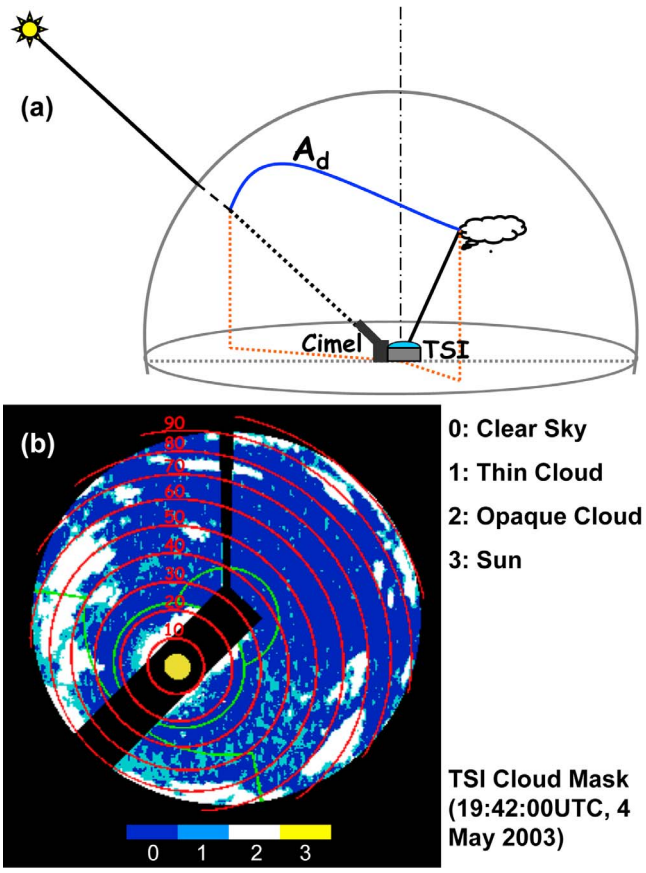

Figure 1. (a) Geometry of observation for the Cimel Sun photometer and for the Total Sky Imager (TSI). A_d stands for an angle between the pixel of the Sun's position and any other pixels in a whole-sky image taken by the TSI. (b) A sample image of cloud mask from TSI. Indices 0, 1, 2, and 3 stand for "clear-sky," "thin cloud," "opaque cloud," and "location of the Sun," respectively. Circumsolar areas for which cloud cover is acquired are presented together with the cloud mask image. Green outlines denote areas where separate cloudy and clear pixel counts are included in the total sky cover data files.

large intensity changes near the Sun's position. Therefore, whenever the intensity becomes larger than the maximum that the CCD camera can handle, bright circumsolar areas appear as white, resulting in a color relationship in that area that is similar to that for clouds [*Long et al.*, 2001]. The cloud cover estimated from the TSI agrees within 5% (10%) with more accurate estimates from a more advanced instrument named the Whole Sky Imager (WSI) [*Long et al.*, 2001] for 87% (94%) of the data under comparison. We assume that the cloud cover from the TSI has an uncertainty level of 5%–10% according to the statistics. While there is lack of in depth characterization of the instruments, we realized that cloud cover estimation is often subject to errors under certain atmospheric conditions, possibly caused by enhanced aureole radiation, which necessitate an in-depth examination on the performance of the TSI cloud mask before the data are utilized for this study.

[12] To this end, we computed the cloud cover for the circumsolar areas with varying angular distances (A_d) from the Sun's position. As shown in Figure 1, A_d was computed for both all pixels composing the TSI image and for the circumsolar area within an angular distance of 10°–20° (area A1; see Figure 2b), 10°–30° (area A1 + A2), 10°–40° (A1 + A2 + A3), and so on. In addition to cloud covers for the different circumsolar areas, we also computed cloud covers for circular areas of the same zenith angles but different azimuth angles at 90° intervals (0°, 90°, 180°, and 270° from the Sun's azimuth angle; see Figure 2a). Much less problem is expected for circular areas in domains 1–3 in Figure 2a.

[13] Assuming that the cloud cover for the four regions defined in Figure 2a should bear statistically equal chances of occurrence, any excessive cloud cover in the circumsolar area (i.e., area with azimuth ID 0) can be considered as an artifact

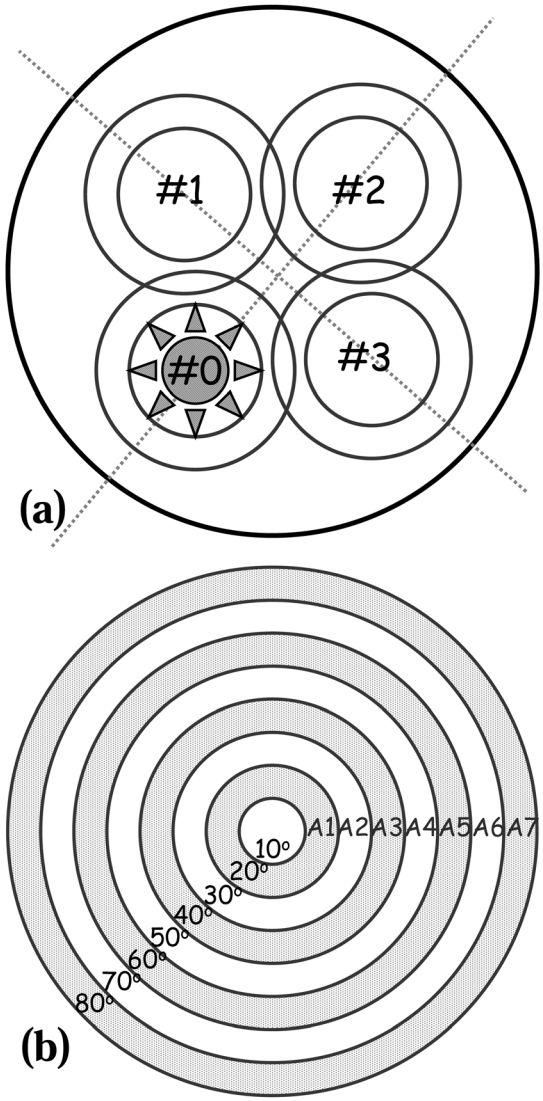

Figure 2. (a) Definition of azimuth ID for computing cloud cover from a TSI cloud mask image. The Sun is located at the center of the area for azimuth ID 0. (b) Definition of circular area (a doughnut shape) over which cloud cover is computed.

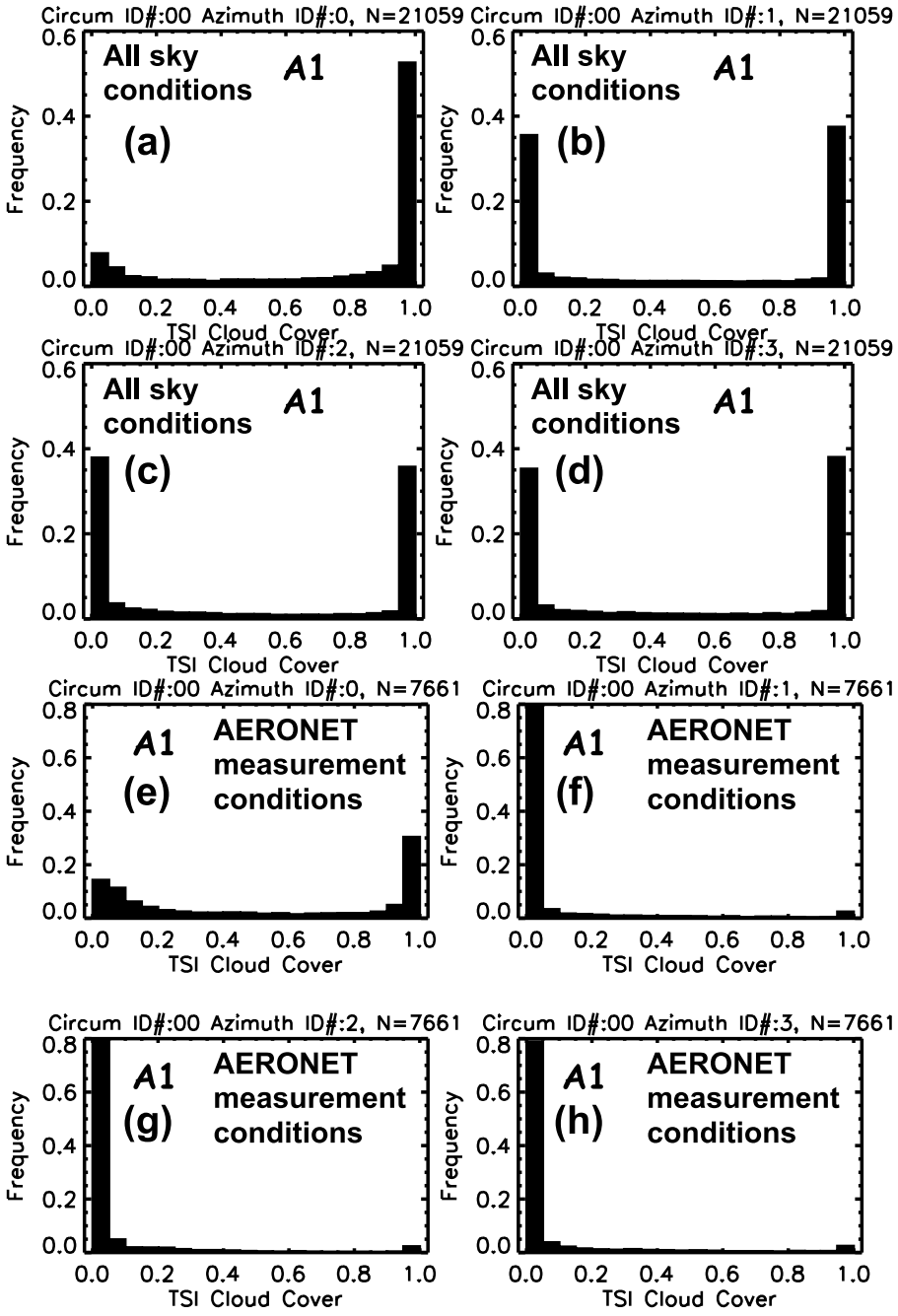

Figure 3. Histograms of TSI cloud cover for inner circular areas with angular distance between 10 and 20° (A1 in Figure 2b) from the center of respective azimuth ID. (a–d) Statistics for all-sky conditions. (e–h) Conditions coincident with the AERONET AOT measurements.

in the cloud cover estimation due to the uncertainty in cloud discrimination near the Sun's position. The values of cloud cover for the innermost circumsolar area (i.e., area A1 in Figure 2b at azimuth ID 0) and for its counterparts at different azimuth sectors (i.e., the areas corresponding to A1 at azimuth IDs 1 through 3) were computed and compared in Figure 3. Figures 3a–3d are histograms of cloud cover under all-sky conditions, representing the four different azimuth sectors (azimuth IDs 0–3). The histograms for the three sectors away from the Sun (azimuth IDs 1–3) are very similar to each other, supporting that the assumption of equal chance of cloud occurrence at any portion of sky with equivalent areas be valid. On the contrary, the cloud cover for the innermost circumsolar area (area A1 at azimuth ID 0) presents very high occurrence (~50%) cloud cover of unity (i.e., 100% of the circumsolar area covered by cloud). Also, the cloud cover for azimuth IDs 1–3 shows ~40% occurrence of cloud-free conditions, while less than 10% occurrence of clear condition

is observed around the Sun (azimuth ID 0). These results suggest that cloud cover from TSI around the circumsolar area tend to be significantly overestimated. Since we are going to match up the cloud cover data with AERONET AOT, TSI cloud mask data coincident with AERONET AOT measurements were collected and the same test was conducted. Figures 3e–3h present results consistent with those for all-sky conditions. Since AERONET AOT is reported only when it is determined to be cloud-free between the Sun photometer and the Sun, the circumsolar area near the Sun (A1 at azimuth ID 0) is expected to contain very low coverage of clouds. Even the other portions of the sky at the time of valid AERONET AOT measurements would have low cloud coverage, as AERONET cloud screening is based on a series of tests utilizing temporal variability over various time periods. From Figures 3e–3h, the regions with azimuth IDs 1–3 show an 80% occurrence of cloud-free skies, while only about 15% occurrence of clear condition is observed around the Sun (azimuth ID 0). A 30% occurrence of very high cloud cover (>0.95) around the Sun indicates that the problems with the TSI cloud cover are very serious in this area. However, this area constitutes a relatively small portion of the whole sky, so the effect on the whole sky cover may be much smaller than shown in Figure 3. Thus, we performed a similar test for larger circular areas with different inner circular areas removed. That is, we computed cloud cover for the areas with a radius between 10°–80°, 20°–80°, 30°–80°, and 40°–80°. Figure 4 shows the comparisons of cloud cover computed for the two areas belonging to two azimuth IDs 0 (i.e., the sector contains the Sun) and 2 (the sector contains a point at the same zenith angle with the Sun but at 180° azimuthal angle difference). It clearly shows that a significant bias exist if the innermost circumsolar areas (10°–30°; A1 and A2) are included in cloud cover calculations. Nearly identical histograms between the two azimuth IDs are obtained when areas A1, A2, and A3 (10°–40°) are excluded.

[14] The results of the tests above suggest that removal of the circum-solar area within a 40° angular radius helps remove the overestimation of TSI cloud cover for the whole sky. However, since such an area occupies a significant portion of the sky and the problem of the TSI cloud mask does not happen all the time, discarding such a large area may result in the loss of much useful data. So we decided to remove the data within 30° of the circumsolar area, instead of 40°, which is a compromise based on Figure 4. For the rest of this study (except for Figure 7), cloudy pixels for circumsolar area within 30° from the center of the Sun's position are removed from the analysis. All the other TSI pixels with zenith angles less than 80° are included in cloud cover calculations. Finally, there might be errors in TSI cloud cover depending on the vertical extent of clouds and viewing angles. We examined this possibility by checking cloud cover within 10° radius centered at the location of the Sun on the TSI mirror (azimuth ID 0), and the other azimuthal areas (IDs 1–3) at a various solar (viewing) zenith angles. The result (not shown here) revealed that angular dependence of the fractional cloud cover is less than 0.1, except for the circumsolar areas (ID 0), where fractional cloud cover error could be as large as 0.6. As the circumsolar areas are removed from the cloud cover to be used for the rest of this study, any residual angular dependence of cloud cover would be small and should retain a negligible influence.

2.3. CART Raman Lidar

[15] The CART Raman lidar (CARL) is a custom-designed instrument developed for the ARM program by the Sandia National Laboratories. CARL is an active, ground-based laser remote sensing instrument that measures the profiles of water vapor, aerosols, and clouds in the troposphere [*Goldsmith et al.*, 1998]. It is composed of a Nd:YAG (yttrium aluminum garnet; $Y_3Al_5O_{12}$) laser that transmits light pulses at 355 nm with 400 mJ at 30 Hz and a receiving telescope of 61 cm diameter. It collects the light backscattered by molecules and aerosols at the laser wavelength and the Raman scattered light from water vapor (408 nm) and nitrogen (387 nm) molecules. The profiles of aerosol backscattering and extinction coefficients, water vapor mixing ratio, and relative humidity are derived on a routine basis using a set of automated algorithms [*Turner et al.*, 2002]. Aerosol scattering ratio profiles can be computed using the Raman scattered light (387 nm) from nitrogen molecules and the backscattered light at 355 nm. Then, the profiles of aerosol backscattering cross sections are computed using the aerosol scattering ratio profile and a molecular scattering cross-section profile derived from a density profile of the atmosphere. Aerosol extinction profiles are then computed by taking the derivative of the logarithm of the Raman scattering signal from nitrogen with respect to the lidar range. Water vapor mixing ratio can be computed by taking the ratio of the Raman scattered signal from water vapor to that from nitrogen molecules. Then, temperature profiles from the Atmospheric Emitted Radiance Interferometer (AERI) are used together with the water vapor mixing ratio profiles to compute the profiles of relative humidity (RH). The accuracies of RH and aerosol extinction profiles are 5% and 10%, respectively [*Turner et al.*, 2002]. Further details are documented by *Ferrare et al.* [2004, 2006] and *Turner* [2004].

2.4. In Situ Aerosol Profiles

[16] Over the SGP site, a light weight aircraft (Cessna C-172N) flew a few times per week to measure profiles of aerosols from March 2000 through January 2006, as a joint effort between the ARM program and the Climate Monitoring and Diagnostics Laboratory (CMDL) of the U.S. National Oceanic and Atmospheric Administration (NOAA). Normally, the aircraft flew at nine level legs between 500 and 4000 m above the ground over the SGP site, measuring the scattering and absorption coefficients for aerosols at 1 Hz sampling rate. The scattering coefficients were measured at three channels (450, 550, and 700 nm) by a nephelometer (TSI 3563) under dry condition (RH ~ 40%) and at a green channel (550 nm) by another nephelometer (Radiance Research Model 903) under humidified conditions (RH ~ 80%). The absorption coefficients were measured only at a green channel by a Particle Soot Absorption Photometer (PSAP; Radiance Research) under low RH levels (~40%). Humidity control system is on board to ensure the desired levels of relative humidity for respective instruments. Further details on the IAP measurements are documented by *Andrews et al.* [2004]. The data were used to study the aerosol humidification effect over the SGP region [*Jeong et al.*, 2007]. In this study, scattering coefficients at ambient RH were calculated using two-parameter function fitting (i.e., humidification factor = $a[1 - \mathrm{RH}]^{-b}$) assuming hygroscopic growth of aerosols [e.g., *Kasten*, 1969; *Hänel*, 1976; *Hegg*

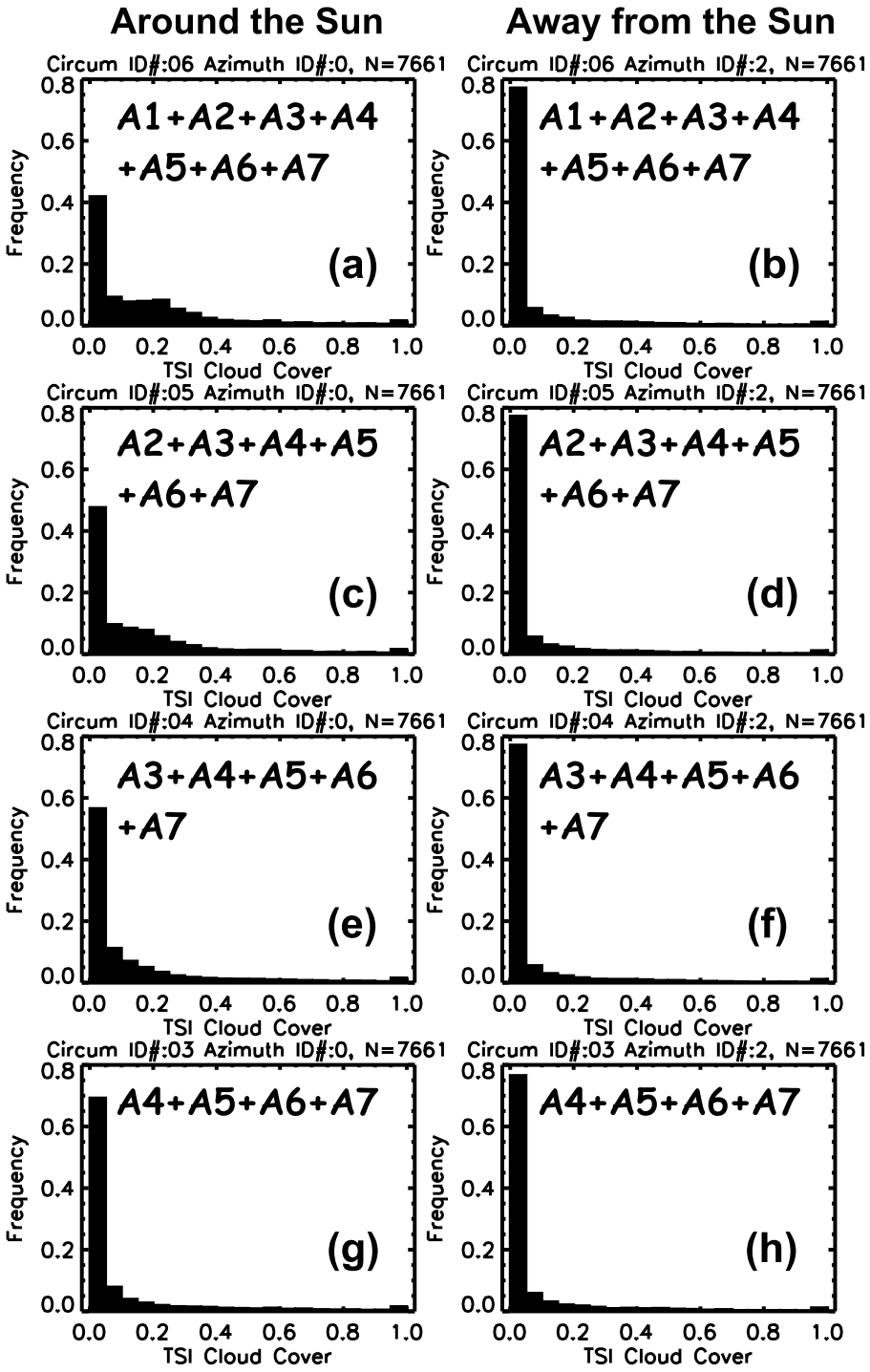

Figure 4. Histograms of TSI cloud cover computed for different inner circular areas (e.g., among a, c, e, and g) and different azimuth domains (e.g., a versus. b; c versus. d).

et al., 1996; *Kotchenruther et al.*, 1999; *Jeong et al.*, 2007] together with the measurements of ambient RH and scattering coefficients at low and high RH levels.

3. Observed Correlation Between AOT and Cloud Cover and Possible Causes

[17] Cloud cover data from the TSI were first coupled with AERONET AOT data, which were only retrieved for clear skies in the direction of the Sun. Then, as many atmospheric variables tend to be autocorrelated, we tried to subsample the coupled data set at a rate of 1/10 to ensure that the selected measurements are statistically independent. As a result, just a few data points were chosen each day for the rest of results shown in this paper. Note that a wider separation of data samples would achieve more statistical independence, but undersampling could result in too few data to offset the statistical significance.

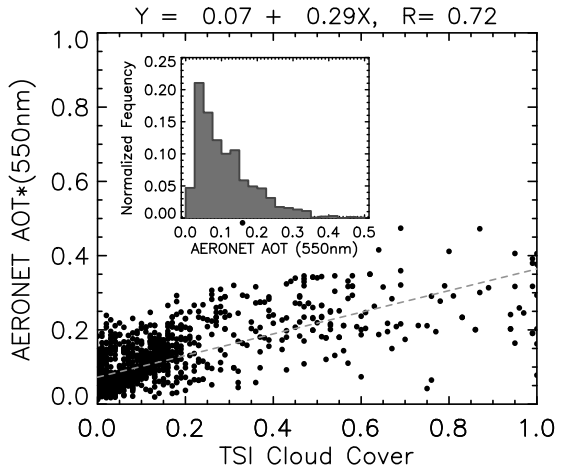

Figure 5. AERONET AOT as a function of cloud cover from TSI. Gray dashed line stands for the least squares fit, and *R* is correlation coefficient. A histogram of AOT used in the scatterplot is presented together. The number of data points is 730.

[18] The AERONET AOT was plotted as a function of the cloud cover in Figure 5. It is clear that the AERONET AOT increases with increasing cloud cover. In addition, the slope is higher than that reported from satellite-retrieved quantities [e.g., *Ignatov and Nalli*, 2002]. For the reasons outlined in section 1, it is very important to understand the causes for the correlation between AOT and cloud cover. In principle, several factors may be at play: (factor a) aerosol humidification effects associated with increasing RH coincident with increasing cloud cover; (factor b) increasing aerosol concentration due to air convergence; (factor c) increasing number of cloud-processed particles; (factor d) new particle genesis near clouds; (factor e) cloud contamination in the AERONET AOT; (factor f) an artifact due to the problem of cloud detection using the TSI; (factor g) increased cloud formation, which could not have occurred without a supply of aerosols; and (factor h) aerosols lengthen the lifetime of clouds, resulting in overall increase in cloud cover. These factors are summarized in Table 1 to help readers navigate through this paper. The factors g and h can be considered as aerosol indirect effects, whereas the others are either real effects or artifacts of clouds on aerosols. The first aerosol indirect effect (i.e., changes in cloud droplet size due to increased aerosol number concentration) could be detectable from such observations as claimed in the literature [e.g., *Feingold et al.*, 2003, 2006; *McComiskey et al.*, 2009]. In this study, however, aerosol indirect effects on cloud cover (i.e., factors g and h) are not considered explicitly because such effects would be realized after a certain time lag which would not be easily detectable in point-wise observations at a fixed location. Besides, the aerosol indirect effect on cloud cover (and its lifetime) is very difficult to measure and its direction would diverge, increase or decrease of cloud cover, depending on conditions such as aerosol absorption property, water vapor supply, or entrainment [e.g., *Koren et al.*, 2004; *Small et al.*, 2009]. In addition, factor g is unlikely to be a main driver of the correlations between aerosol optical thickness and cloud cover as the aerosol burden at the SGP site is usually sufficient to foster cloud formation, while we cannot completely rule out the possibility of aerosol indirect effects at play. In the following sections, the effects of the other factors related to clouds on the observed apparent correlation between cloud cover and AOT are examined in detail. Aerosol indirect effects on cloud cover will be attributed to the factors possibly contributing to the unresolved portion of the correlations between AOT and cloud cover.

4. Examination and Discussion

4.1. Effect of the Uncertainty in the Cloud Cover Estimations

[19] Given the difficulties to discriminate clear and cloudy skies around the Sun's position as discussed in section 3, it is necessary to assure if the correlation shown in Figure 5 is an artifact or not. In addition, it is important to check the effects of our exclusion of data within innermost circumsolar area (<30°) for TSI cloud cover derivation. To this end, we correlated the cloud cover derived for the circumsolar areas with various angular distances (A_d) from the Sun's position (see Figure 1) with the AERONET AOT (Figure 6). The results show that the correlations between AERONET AOT and TSI cloud cover exist for all the circumsolar areas. The correlation coefficient (*R*) for the different circumsolar areas is rather similar (0.68–0.76), while the slopes increase as the circumsolar area increases (from 0.16 to 0.29). It is evident that the AERONET AOT has a stronger relationship with cloud cover, in terms of both slope and correlation coefficients, as the circumsolar area increases. These results indicate that the correlation between AERONET AOT and TSI cloud cover is not an artifact due to the problem of the TSI cloud mask. Otherwise, steeper slopes would have been found for the inner circumsolar areas because the enhanced aureole radiation by aerosol scattering would cause more difficulty in

Table 1. Possible Causes of Correlation Between Aerosol Optical Thickness (AOT) and Cloud Cover

Factor	Possible Causes	Remark
a	Aerosol humidification effect	Real effect[a]
b	Atmospheric convergence	Real effect
c	Cloud-processed particles	Real effect
d	New particle genesis	Real effect
e	Cloud contamination in observed AOT	Artifact; possible both in ground- and satellite-based observations
f	Erroneous cloud detection	Artifact; possible both in ground- and satellite-based observations
g	Increased cloud formation with a supply of aerosols	Real effect; aerosol indirect effect
h	Lengthened lifetime of cloud due to increased aerosol loading	Real effect; aerosol indirect effect
NG[b]	Enhanced scattering or absorption of photons near clouds	Artifact; possible in satellite observations

[a]Real effect can be found both in ground- and satellite-based observations.
[b]NG: factor is not given as it is relevant only to satellite-based observations, which are not covered in this study.

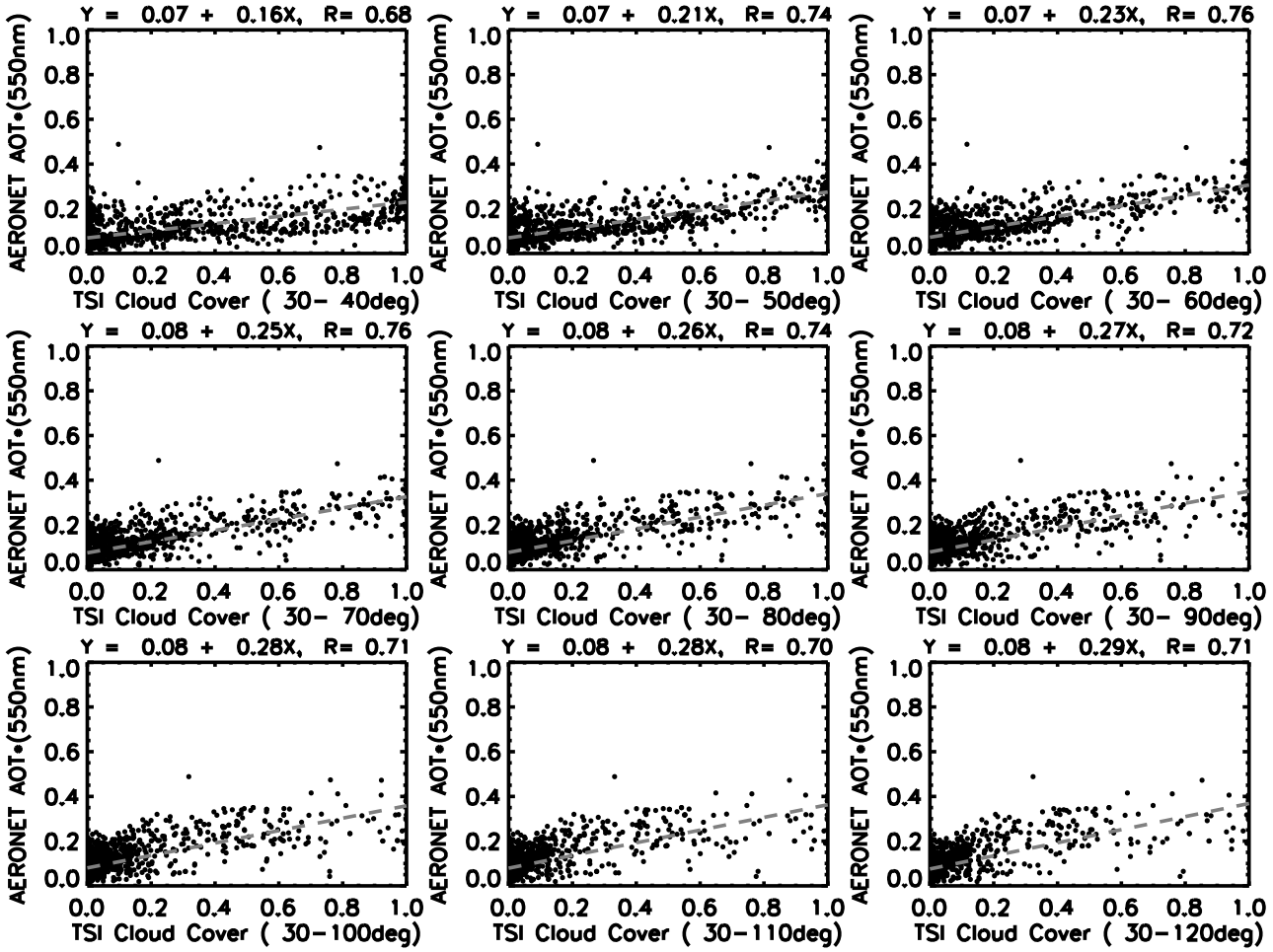

Figure 6. Scatter plots of AERONET AOT as a function of TSI cloud cover for the circumsolar areas within different angular distances from the line of sight to the Sun.

discriminating cloud from the clear sky. On the other hand, the increasing slopes with increasing circumsolar areas may imply that the effects of cloud cover are related to increasing AHE, convergence, or processed/new particles. These effects would not significantly depend on the local clouds around the Sun.

[20] Given the compromise we made regarding the cutoff angle for computing cloud cover, there might be a remaining artifact in the TSI cloud cover even after the correction. So we checked further if there is any dependence of the AOT-cloud cover correlation on the area of the inner circumsolar region discarded for the TSI cloud cover correction. In Figure 7, the cloud cover for Figure 7a was computed for a circumsolar area within 10°–50°, Figure 7b within 20°–50°, Figure 7c within 30°–50°, and Figure 7d within 40°–50°. Note that both the slopes and R showed little change after the data within innermost circumsolar area were excluded for the TSI cloud cover derivation. The changes in slopes (~0.04) and offsets (~0.02) may be construed as an indicator of uncertainties associated with residual errors of TSI cloud cover that might affect the relationship between TSI cloud cover and AERONET AOT. We also investigated cases with different circumsolar areas removed from large sky areas (e.g., areas within 60°, 70°, 80°, and 90° from the location of the Sun) to check if the variability of the slopes and offsets changes with the sky area for which cloud cover is calculated. The results (not shown) indicate that the variability does not change significantly from that shown in Figure 7. For instance, the differences of slopes between the cases with circumsolar areas of 10°, 20°, 30°, and 40° removed from the whole-sky area are very similar (~0.01) in comparison to ~0.04 as shown in Figure 7. On the basis of Figure 4 together with visual examinations of the individual images of sky and cloud mask, it is concluded that the TSI cloud masking is rarely affected by intense aureole radiation for angular distances greater than 40° except for large solar zenith angles (e.g., >70°). Therefore, we do not expect a significant correlation due to the erroneous TSI cloud mask in Figure 7d. Thus, the rather invariant slopes, intercepts, and R in Figure 7 indicate that the correlation between AERONET AOT and TSI cloud cover is not affected by the problem of the TSI cloud masking near the Sun's position.

4.2. Effect of Relative Humidity

[21] Having shown that the AOT-cloud cover correlation does not originate from an artifact in the TSI cloud cover estimation (factor f in Table 1), the remaining major possibilities are the AHE (factor a), convergence (factor b), and cloud-processed particles (factor c), and new particle genesis (factor d). First, we try to examine the relationship between

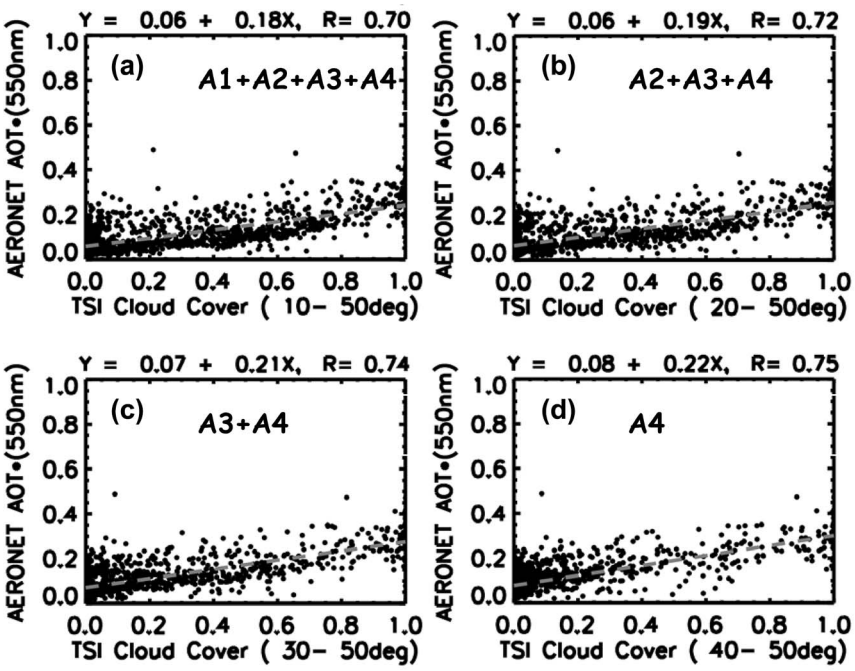

Figure 7. AERONET AOT as a function of the TSI cloud cover for circumsolar areas with angular distance from the Sun's position (a) between 10° and 50°, (b) 20°–50°, (c) 20°–40°, and (d) 40°–50°.

cloud cover, RH, and AOT. Figure 8 shows AERONET AOT as a function of (1) TSI cloud cover (top) and (2) aerosol extinction weighted column mean RH, ⟨wRH⟩ (middle), ⟨wRH⟩ as a function of TSI cloud cover is also shown (bottom). Linear regression analysis is done as shown in Figure 8, and corresponding standard errors of the slopes and offsets are provided in Table 2. ⟨wRH⟩ was introduced by *Jeong et al.* [2007] to parameterize AHE and is defined as follows,

$$\langle \mathrm{wRH} \rangle \equiv \int_{z1}^{z2} k_{\mathrm{ext}}^{\mathrm{a}}(\mathrm{RH}, z) \cdot \mathrm{RH}(z)\mathrm{d}z \Big/ \int_{z1}^{z2} k_{\mathrm{ext}}^{\mathrm{a}}(\mathrm{RH}, z)\mathrm{d}z. \quad (1)$$

⟨wRH⟩ was calculated using the profiles of RH and aerosol extinction ($k_{\mathrm{ext}}^{\mathrm{a}}$) from the Raman lidar. Figures 8a and 8b show that there is a correlation between AERONET AOT and ⟨wRH⟩, albeit weaker than the one between AOT and cloud cover. Figure 8c also shows there is a correlation between cloud cover and ⟨wRH⟩. Interestingly, the correlation between AOT and cloud cover is strongest among the three-way comparisons of the variables. This finding indicates that a cloud cover increase is somewhat related to, but not necessarily always accompanied by, an increase in column RH or vice versa, under meteorological conditions for which AERONET AOT can be obtained. Similarly, AOT is related to ⟨wRH⟩ to a certain degree but is not dominated by changes in ⟨wRH⟩. Thus, the comparable correlations of the two variables with AOT are likely to be associated with different factors. At this point, we speculate that cloud-processed particles (and new particles) may be related to the correlation between AOT and cloud cover, while the AHE is partially linked to the correlation between AOT and ⟨wRH⟩. Both correlations may be associated with a third variable such as air convergence that can cause increases in cloud cover, aerosol, and water vapor.

[22] Typically, it is very difficult to determine the contribution of the AHE to the AERONET AOT since it requires vertical profiles of RH and aerosol properties (e.g., profiles of aerosol scattering and absorption coefficients at an ambient, low RH). *Jeong et al.* [2007] showed that the AHE over the ARM SGP site can be represented as a function of column mean RH. We use aerosol extinction weighted column mean RH, ⟨wRH⟩, the column aerosol humidification factor (AHF; also denoted as R(RH)) and the AHE as defined in equations (2) and (3),

$$R(\mathrm{RH}) \equiv \tau_{\mathrm{sca}}^{\mathrm{a}}(\mathrm{RH})/\tau_{\mathrm{sca}}^{\mathrm{a}}(40\%), \quad (2)$$

$$\mathrm{AHE} \equiv \frac{\tau_{\mathrm{sca}}^{\mathrm{a}}(\mathrm{RH}) - \tau_{\mathrm{sca}}^{\mathrm{a}}(40\%)}{\tau_{\mathrm{ext}}^{\mathrm{a}}(\mathrm{RH})}, \quad (3)$$

where $\tau_{\mathrm{sca}}^{\mathrm{a}}$ and $\tau_{\mathrm{ext}}^{\mathrm{a}}$ are AOT, respectively, due to scattering and extinction (scattering + absorption), which are dependent on RH. By combining equations (2) and (3), the AHE can be rewritten as

$$\mathrm{AHE} = \frac{R(\mathrm{RH}) - 1}{R(\mathrm{RH}) - 1 + 1/\omega_0}, \quad (4)$$

where ω_0 is the column mean single scattering albedo at a dry condition (RH ~ 40%). We use the aerosol extinction at 355 nm, RH profiles derived from the Raman lidar [*Turner et al.*, 2002] and the parameterized relationship between ⟨wRH⟩ and R(RH), which was proposed by *Jeong et al.* [2007] (Method 1 as described in their Table 2). The AHE can be inferred from equation (4) with R(RH) calculated from Raman lidar observations. The single scattering albedo is 0.95, which is the average observed from the AOS at the SGP site [*Sheridan et al.*, 2002]. The AHE is not very sensitive to

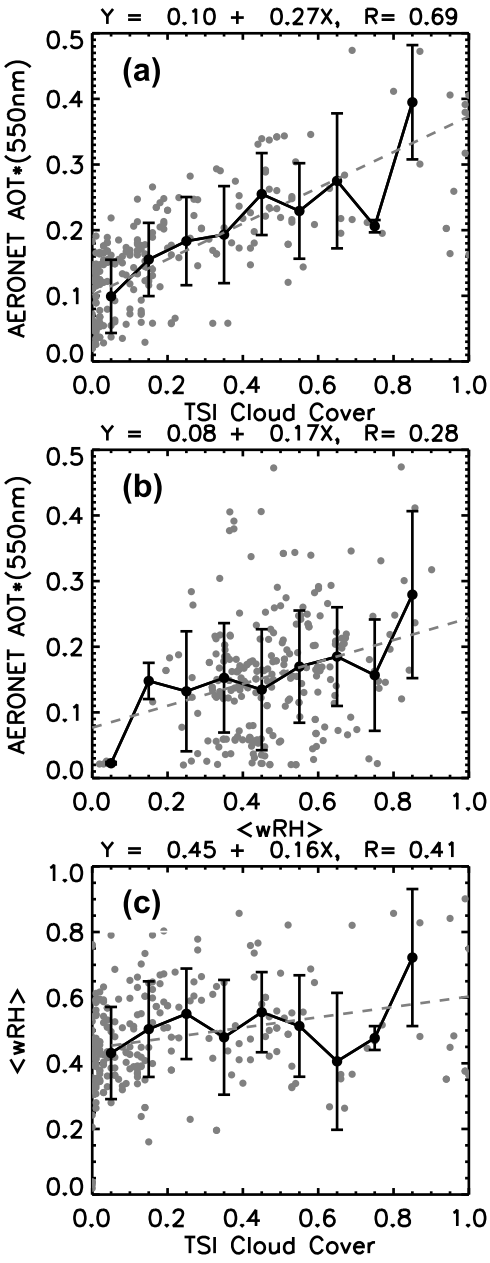

Figure 8. (a) AERONET AOT as a function of TSI cloud cover, (b) AERONET AOT as a function of aerosol extinction weighted column mean RH ⟨wRH⟩, and (c) ⟨wRH⟩ as a function of TSI cloud cover. Gray symbols are individual observations. Gray dashed lines represent respective linear regression lines derived using individual data points. Binned averages and standard deviations are shown in black symbols and lines.

realistic values of the single scattering albedo for $R(\mathrm{RH}) < 3$, which is typical over the SGP site [*Jeong et al.*, 2007]. Estimations of the AHE using this method may be subject to errors due to the variability of the aerosol hygroscopicity since the methodology is based on the average connectivity between aerosols and RH (i.e., ⟨wRH⟩) over the SGP site. A large amount of data are available from the Raman lidar, a statistically significant number of match-ups with AERONET and TSI measurements can be obtained, enabling the examination of the statistical relationship between AOT and cloud cover. The contributions of the AHE to the AERONET AOT and the AERONET AOT without the AHE are shown in Figure 9. The AOT due to the AHE is nearly zero for ⟨wRH⟩ less than 40% and sharply increases for ⟨wRH⟩ greater than 80%. From Figure 8b and Figure 9a, it can be seen that the AHE contributes up to roughly 50% of the AOT at ⟨wRH⟩ = 0.8 compared to dry conditions (⟨wRH⟩ = 0.4). A range of errors that might exist in the estimations of AHE (reported by *Jeong et al.* [2007]) is also provided in

Table 2. Coefficients and Associated Standard Errors of Linear Regressions Between Aerosol Optical Thickness (AOT), Cloud Cover, and Aerosol Extinction Weighted Column Mean Relative Humidity (⟨wRH⟩)[a]

	Intercept	Slope
Figure 8a	0.101 (±0.005)	0.272 (±0.015)
Figure 8b	0.077 (±0.017)	0.167 (±0.035)
Figure 8c	0.446 (±0.012)	0.157 (±0.037)
Figure 10a	0.007 (±0.003)	0.060 (±0.009)
Figure 10b	0.096 (±0.005)	0.203 (±0.015)

[a]Numbers in parentheses are standard errors. All the linear regressions presented here are statistically significant at the confidence level of 95%.

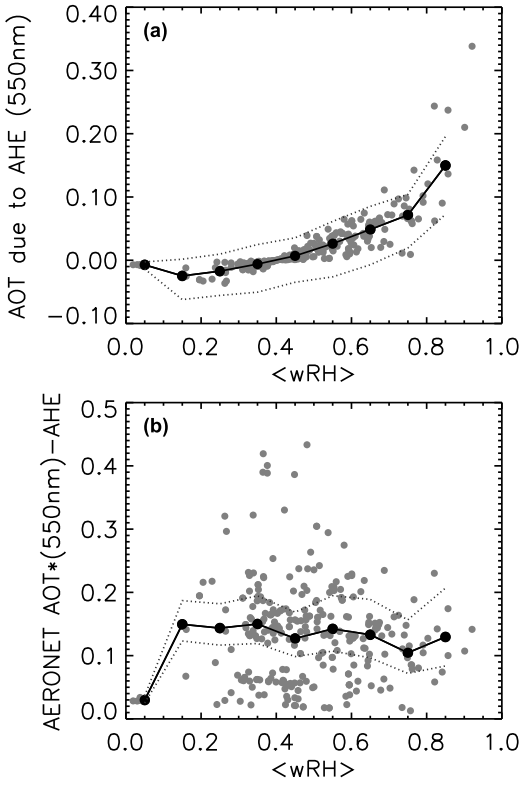

Figure 9. (a) AERONET AOT due to the aerosol humidification effect (AHE) as a function of ⟨wRH⟩. (b) Same as in Figure 9a, but for AERONET AOT when contributions of AHE are removed. Gray symbols are individual observations. Binned averages are shown in black symbols with solid lines. Dotted lines indicate the ranges of uncertainty for binned averages of AOT due to AHE and AHE-removed AOT, which are calculated from the AHE uncertainty range reported by *Jeong et al.* [2007].

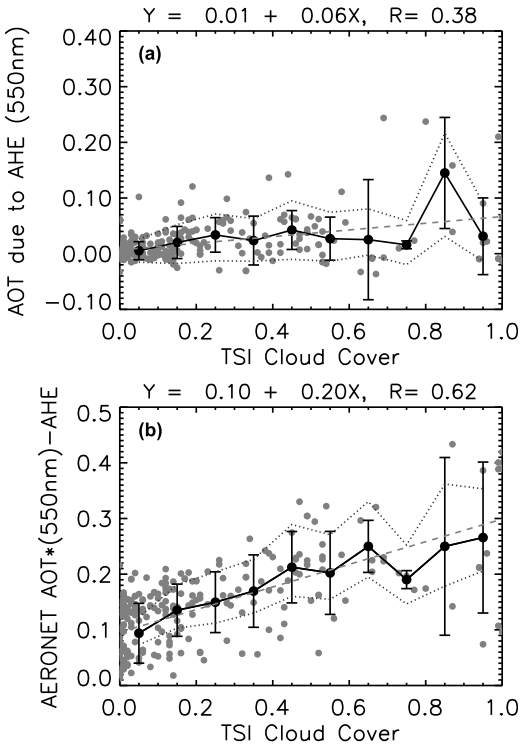

Figure 10. (a) AERONET AOT due to AHE as a function of TSI cloud cover. (b) Same as in Figure 10a, but AERONET AOT without AHE. Gray symbols are individual observations, and binned averages are shown in black symbols with solid lines. Gray dashed lines represent respective linear regression lines derived using individual data points. Dotted lines indicate the ranges of uncertainty for the binned averages due to the uncertainty in the AHE derivations.

Figure 9. The impact of such uncertainty in the conclusions of this study will be discussed in section 4.5. Figure 9b shows estimations of the AERONET AOT with the AHE contribution removed. It is obvious that the AOT dependence on ⟨wRH⟩ disappears when the AHE is removed from the AERONET AOT. Note that the parameterization of the AHE as function of ⟨wRH⟩ was derived solely from the IAP observations and is independent from the AERONET and Raman lidar measurements.

[23] Having successfully removed the AHE from the AERONET AOT, the AOT due to the AHE, and without the AHE are correlated with the TSI cloud cover in Figure 10. The associated error ranges of slopes and intercepts are provided in Table 2. Interestingly, both AOT show a significant correlation with the cloud cover. However, the slope for the AOT due to the AHE (0.06) is roughly one third of that for the AERONET AOT without the AHE (0.20). This result shows that the AHE contributes about one fourth of the slope (0.06/0.27 ≈ 1/4) for the AERONET AOT and TSI cloud cover relationship.

4.3. Effects of Cloud-Processed Aerosols and New Particle Genesis

[24] Two of the remaining major factors to possibly explain the correlation between the cloud cover and AOT, cloud-processed aerosol particles (factor c) and newly generated particles (factor d) under a humid environment near clouds [*Hoppel et al.*, 1990; *Hegg et al.*, 1990; *Hoppel et al.*, 1994; *Alkezweeny*, 1995; *Hegg et al.*, 2004] are discussed in this section. Here cloud-processed particles are meant to be aerosols left after cloud droplets evaporate. For instance, an entrainment of dry air to the edges of clouds can result in evaporation of cloud droplets, leaving interstitial and in-droplet aerosol particles behind. An order of 10% increase of aerosol scattering efficiency due to cloud processing of aerosols was reported [*Hegg et al.*, 2004]. On the other hand, new particle genesis is in reference to homogenous and heterogeneous nucleation such as sulfate production through a gas-to-particle conversion [e.g., *Hoppel et al.*, 1990; *Alkezweeny*, 1995].

[25] Four sets of aerosol extinction profiles obtained from the IAP and the AOS are shown in Figure 11. In each set of measurements, two aerosol extinction profiles (for particle diameter, Dp < 1 μm at ambient RH, and for Dp < 1 μm at RH = 40%) are shown in Figure 11. In Figure 11, occasional measurements of extinction coefficients at ambient RH fall below those for RH = 40% are likely due to uncertainties in measurements under very low aerosol loading, especially for the wet nephelometer (Radiance Research M903). Aerosol extinction profiles at ambient RH are presented together with those at a fixed RH (40%) to separately show the AHE and non-AHE. It should be noted that the peaks of aerosol extinction profiles at RH = 40% in Figure 11, nothing to do with AHE, coincide with the altitudes of cloud layers (see cloud bottom altitude information in Figure 11). For instance, on 7 May in Figure 11a, the largest peak of aerosol extinction is located right below the bottom of the cloud layer (and extinction increasing inward the cloud layer). Also, for the other cases (i.e., on 13 May; also on 21 and 22 May in Figure 11; and many other IAP observations), the aerosol extinction maxima coincide with the altitudes of cloud layers. Considering that the AERONET AOT observations with moderate aerosol loading are made under the presence of sparse or dissipating clouds (e.g., Table 3; visual inspection of TSI images), those collocated peaks of aerosol extinction profiles with cloud layer, rather than those for atmospheric convergence (not shown here), can be an indication of residual particles left by dissipated clouds or new aerosol particle genesis under a humid environment near edges of clouds.

4.4. Examination on the Correlation Between AOT and Cloud Cover Using in Situ Aerosol Measurements

[26] As a cross check, AOT derived from the IAP measurements is examined if it is also correlated to the cloud cover derived from the TSI. Since RH is controlled during the IAP measurements and the measurements are not subject to cloud contamination (factor e), the effects of atmospheric convergence (factor b), cloud-processed particles (factor c), or new particle genesis (factor d) can influence the relationship between aerosols and cloud cover. To be correlated with cloud cover, the scattering and absorption coefficients at 550 nm and at a low RH (~40%) from the IAP were vertically integrated using a simple trapezoidal scheme as exercised by *Jeong et al.* [2007]. Comparisons between the IAP AOT at low RH for aerosol particles less than 1 μm in diameter and the AERONET AOT are shown in Figure 12. The two AOTs are well correlated each other but, obviously, there is systematic differences between them, which originates from the

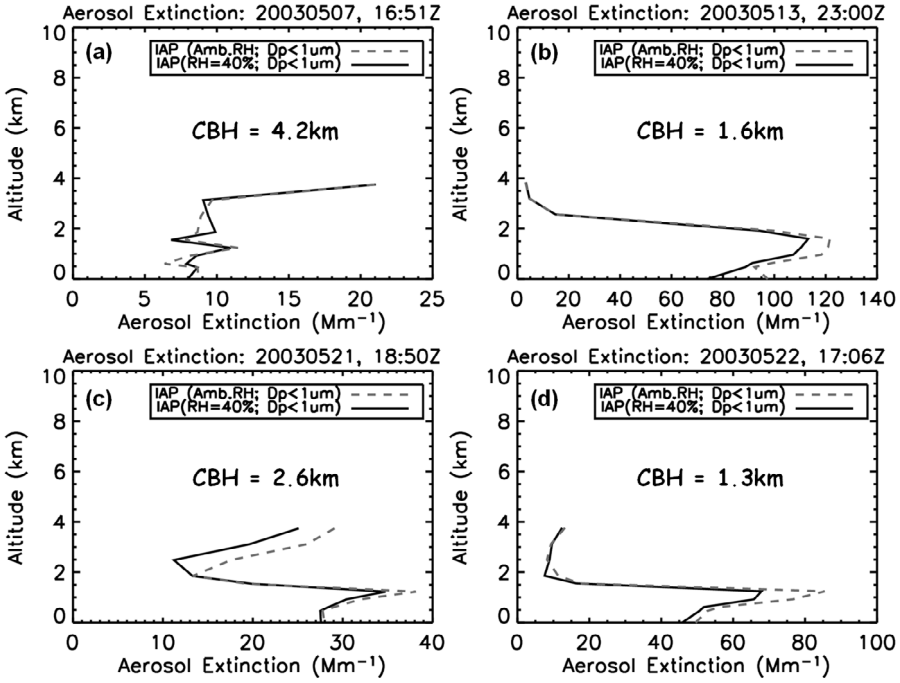

Figure 11. (a) Aerosol extinction profiles from IAP on 7 May 2003. Aerosol extinction profiles for submicron particles (Dp < 1 μm) at ambient RH and RH = 40% are shown in gray dashed and black solid lines, respectively. CBH stands for cloud bottom height. (b) Same as in Figure 11a, but data for 13 May 2003. (c) Same as in Figure 11a, but for 21 May 2003. (d) Same as in Figure 11a, but for 22 May 2003.

missing contributions of the AHE, supermicron-sized particles and aerosols above the highest level leg in the IAP measurements. We adjusted the IAP AOTs for Dp < 1 μm to that for Dp < 10 μm in order to make the IAP AOT comparable with the AERONET AOT as detailed by *Jeong et al.* [2007]. In brief, the adjustment utilizes scattering and absorption coefficients measured with two different size cutoffs (i.e., Dp < 1 μm and Dp < 10 μm) from the Aerosol Observing System at the surface, and the ratios of the coefficients with different size cutoffs at the surface are assumed to be held throughout the column of the atmosphere. The resulting AOT may be overestimated because large particles tend to reside in the lower portion of the atmosphere unless there are large dust particles aloft [*Andrews et al.*, 2004]. Thus, we believe that the true IAP AOT values lie somewhere between the IAP AOTs for Dp < 1 μm and for Dp < 10 μm. The coincident AERONET AOT and IAP AOTs for Dp < 1 μm and for Dp < 10 μm are plotted as functions of the TSI cloud cover in Figure 12. The three AOTs are correlated with the cloud cover but showing slightly different slopes, intercepts, and correlation coefficients (R). The AERONET AOT has the highest slopes (0.24) and R (0.63), which is expected since the AERONET AOT may be additionally affected by the AHE and cloud contamination that do not affect the IAP AOTs. As mentioned above, the true IAP AOT values without the AHE would be somewhere between the IAP AOTs before and after the size adjustment, considering supermicron particles.

[27] The correlations between IAP AOTs and TSI cloud cover reflect the effects of convergence (factor b), cloud-processed particles (factor c), or new particles (factor d). As the AHE contributes to about a quarter (in slope) of the correlation between AERONET AOT and cloud cover (Figures 8a and 10), the true slope for dry conditions would be around 0.18 (= 0.24 × 3/4) if there is no effect of cloud contamination on the AERONET AOT. Thus, we infer that the effects of convergence (factor b), processed particles (factor c), and new particle genesis (factor d) contribute more than half (0.14–0.22 compared to the AERONET AOT's 0.24; possibly three fourth) of the slope of the AERONET

Table 3. Sky Conditions for the Cases Shown in Figure 11[a]

Date	Cloud Cover[b]	Cloud Bottom Height[c]	Remark
7 May 2003	0.4	4.2 km (Cu) 7.2 km (Ac)	Sparse low cloud (Cu), Ac dominant
13 May 2003	0.1	1.6 km (Cu) 11.3 km (Ci)	Dissipating small clouds
21 May 2003	0.9	2.6 km (Sc)	Nearly overcast
22 May 2003	0.1	1.3 km (fair weather Cu)	Repetitive generation/dissipation of clouds

[a]Ac, Cu, Ci, and Sc stand for altocumulus, cumulus, cirrus, and stratocumulus, respectively.
[b]Cloud cover in fraction unit (i.e., overcast is 1.0) obtained from ARM SGP Meta Data System (MDS; available at http://www.db.arm.gov/cgi-bin/MDS/Search.pl).
[c]Cloud bottom height from ARSCL based on micropulse lidar (MPL).

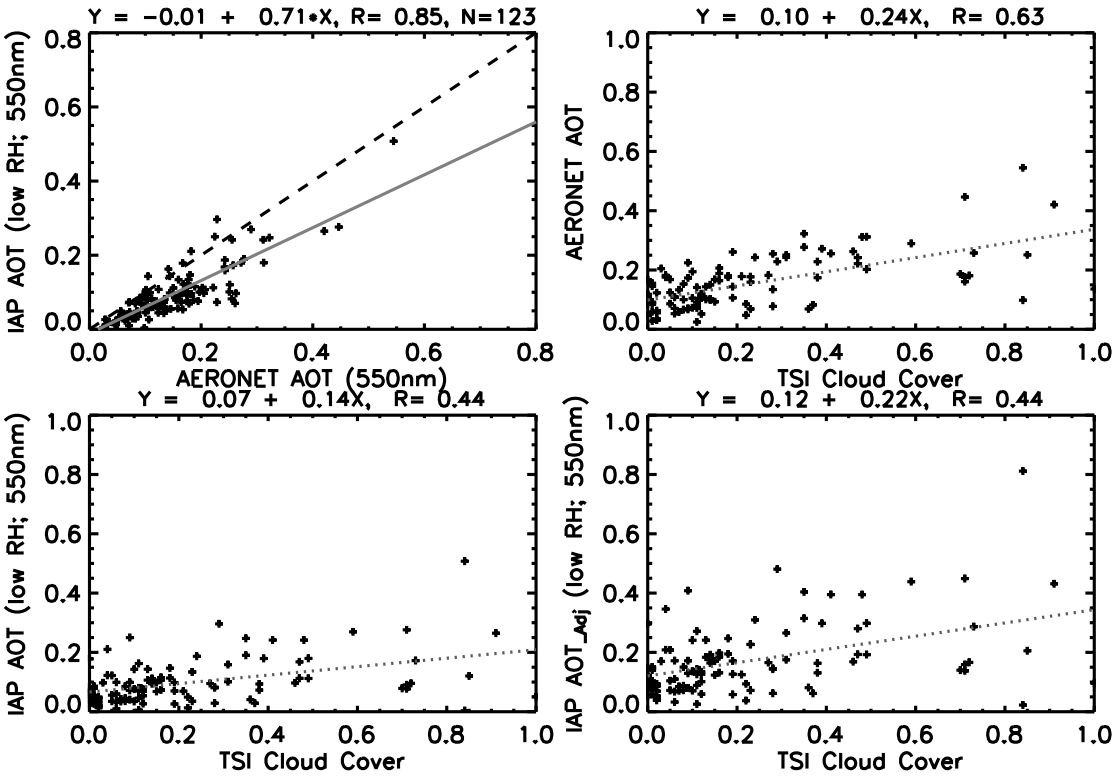

Figure 12. (a) Comparison of the IAP AOT at low RH (~40%) with Dp < 1 μm and AERONET AOT. Black dashed and gray solid lines represent one-to-one and linear regression lines, respectively. (b) AERONET AOT coincident with IAP observations as a function of TSI cloud cover. (c) IAP AOT for particles diameter less than 1 μm (Dp < 1 μm), and (d) IAP AOT after aerosol size adjustment to be compatible to AOT for Dp < 10 μm as functions of TSI cloud cover, respectively. Gray dotted lines stand for linear regression lines.

AOT/TSI cloud cover relationship. By the same token, the contributions of aerosol humidification and cloud contamination are expected to be smaller than half of the slope, and cloud contamination, if any, should be less than 0.05 (<20%).

4.5. Discussions

[28] As discussed in section 2, any cloud contamination that may exist in the AERONET AOT would be due to thin, steady clouds (mostly thin cirrus clouds according to our visual examination on sky images), while the TSI cloud mask also often fails to detect such thin clouds. Therefore, such thin clouds do not contribute to increase in cloud cover detected by TSI cloud masking algorithm. In order for an artifact of thin cirrus clouds to play a role, cloud optical thickness (COT) of such thin clouds should be increased with increasing TSI cloud cover, which is not likely the case as it should be accompanied by the persistent, very thin clouds that were not detected by the AERONET cloud-screening algorithm. Anyway, to check this possibility, we tried to correlate cloud fraction and cirrus reflectance from Moderate Resolution Imaging Spectroradiometer (MODIS) over the SGP site, but no correlation was found. Therefore, we believe that cloud contamination is not likely the major contributor to the observed correlation between the AERONET AOT and TSI cloud cover. Discussions in section 4.4 with IAP measurements also suggest that cloud contamination in AERONET AOT, if any, should be small.

[29] In section 4.2, it was shown that AHE contributes roughly one fourth of the slope between TSI cloud cover and AERONET AOT. It would be necessary to discuss how the reported the range of uncertainty in the AHE estimation by *Jeong et al.* [2007] can influence the conclusion of this study. In Figure 10, the range of AHE uncertainty is provided (dotted lines), which results in a range of slope 0.02–0.11 for AOT due to AHE as function of TSI cloud cover. Thus, the contribution of AHE could be as small as 1/15 or as large as one third. Interestingly, this range is comparable to the differences of the slopes between AERONET AOT-TSI cloud cover pair and IAP AOT-TSI cloud cover pairs (with different size cutoffs) shown in Figure 12. However, as was argued in the previous subsection, the "true" IAP AOT (representing dry particles) values that could have been obtained if there were no size cutoff in the IAP measurements would be in between IAP AOT for Dp < 1 μm and IAP AOT for Dp < 10 μm. Thus, "true" IAP AOT would yield a slope between 0.14 and 0.22, which makes its slope difference from AERONET AOT-TSI cloud cover pair closer to the estimated contribution (slope of 0.06) of AHE reported in section 4.2. This gives us a bit more confidence on our estimation of the AHE contribution, whereas we acknowledge that there exists nonnegligible uncertainty in the estimated contribution of AHE on the AOT-cloud cover slope.

[30] Unfortunately, we are unable to completely separate the effects of atmospheric convergence (factor b), cloud

processed particles (factor c), and new particle genesis (factor d), besides aerosol indirect effects (factors g and h), within the scope of this study, which would require very accurate and extensive measurements of aerosol sizes and chemical substances together with modeling of aerosols' temporal evolutions under cloudy conditions. Nevertheless, the large contributions (about three fourth) of these factors, reported in this study, clearly warrant extensive observation and modeling efforts to facilitate our understanding of the links between clouds and aerosols.

5. Summary and Conclusion

[31] Correlation has been found between aerosol optical thickness (AOT) and cloud cover. For aerosol indirect studies, it is crucial to understand if such correlations are true reflection of their relationships, false manifestation of artifacts, or both. While most studies reporting such relations are based on satellite remote sensing data, they are inherently difficult to sort out the true relation from artifacts. By using much more comprehensive observation data from the Atmospheric Radiation Measurement (ARM), we first report that AOT is indeed correlated with cloud cover using the AERONET AOT data and cloud fraction estimated from the total sky imager (TSI). The causes of the apparent correlation between AOT and cloud cover are painstakingly investigated using a wide variety of measurements made from ground and airborne sensors deployed at ARM South Great Plains (SGP) CART site. It is found that the correlation stems from a combination of factors such as cloud contamination, aerosol humidification, air convergence, cloud-processed or new particles formation (in the presence of clouds), to a varying degree.

[32] Analyses of AERONET AOT, TSI cloud cover, CART Raman lidar, and IAP data reveal that the aerosol humidification effect (AHE) contributes about one fourth to the observed correlation between AERONET AOT and TSI cloud cover. The influence of cloud contamination is expected to be small. Atmospheric convergence seems to play a significant role in determining the vertical distribution of aerosols, while its contribution to the AOT-cloud cover correlation is not obvious. The AOT derived from the IAP measurements, which is not affected by cloud contamination nor by aerosol humidification, is also correlated with cloud cover, suggesting the contributions from cloud-processed particles and new particles near clouds and/or under humid environment. Contributions of such factors seem to reach as large as the three fourth of the slope between cloud cover and AOT. While we are unable to completely separate the effects of convergence and cloud-processed particles and new particles, the correlation between AOT and cloud cover from ground-based measurements (i.e., AERONET and TSI) over the ARM SGP site is mainly due to real effects: the AHE (factor a), convergence (factor b), cloud-processed (factor c), and newly generated particles (factor d). We speculate that aerosol indirect effects on cloud cover (factors g and h) would not significantly influence on the observed correlation, although we cannot completely rule out their possibility. Thus, it would be rather safe to include aerosol indirect effects as contributing factors to the unresolved three quarters of the slope between AOT and cloud cover.

[33] Contrary to the results and conclusions above, it should be noted that any correlation between satellite-based AOT and cloud fraction is likely to be influenced by artifacts such as cloud contamination and cloud adjacency effect (also known as three-dimensional cloud effect). Therefore, caution and more in-depth investigations are necessary to utilize satellite-based AOT for studies on cloud-aerosol interactions in the vicinity of clouds. Also, a sophisticated model with a built-in aerosol/cloud microphysics and associated transport/chemistry will be helpful to tackle the issue.

[34] **Acknowledgments.** The data used in this study were obtained from the Atmospheric Radiation Measurement (ARM) Program sponsored by the U.S. Department of Energy, Office of Science, Office of Biological and Environmental Research, Climate Change Research Division. We thank Dr. Rick Wagener and Dr. Brent Holben for their effort in establishing and maintaining the "Cart_Site" and "CART_SITE" for the AERONET. We are also grateful to the National Oceanic and Atmospheric Administration (NOAA), Climate Monitoring and Diagnostics Laboratory (CMDL), Aerosols Group for providing In Situ Aerosol Profiles (IAP) data sets. We sincerely thank the anonymous reviewers for their careful and constructive comments. This work is supported by the U.S. DOE ARM program grant DE-FG02-01ER63166 managed by Dr. Wanda Ferrell. The study was funded by the DOE/ARM Program (DEFG0208ER64571), NASA Radiation Science Program (NNX08AH71G), and MOST's National Basic Research Program (2008CB403706).

References

Alkezweeny, A. J. (1995), Field observations of in-cloud nucleation and the modification of atmospheric aerosol size distribution after cloud evaporation, *J. Appl. Meteorol.*, *34*, 2649–2654.

Andrews, E., P. J. Sheridan, J. A. Ogren, and R. Ferrare (2004), In situ aerosol profiles over the Southern Great Plains cloud and radiation test bed site: 1. Aerosol optical properties, *J. Geophys. Res.*, *109*, D06208, doi:10.1029/2003JD004025.

Eck, T. F., B. N. Holben, J. S. Reid, O. Dubovik, A. Smirnov, N. T. O'Neill, I. Slutsker, and S. Kinne (1999), Wavelength dependence of the optical depth of biomass burning, urban, and desert dust aerosols, *J. Geophys. Res.*, *104*(D24), 31,333–31,349, doi:10.1029/1999JD900923.

Eck, T. F., et al. (2005), Columnar aerosol optical properties at AERONET sites in central eastern Asia and aerosol transport to the tropical mid-Pacific, *J. Geophys. Res.*, *110*, D06202, doi:10.1029/2004JD005274.

Feingold, G., W. L. Eberhard, D. E. Veron, and M. Previdi (2003), First measurements of the Twomey indirect effect using ground-based remote sensors, *Geophys. Res. Lett.*, *30*(6), 1287, doi:10.1029/2002GL016633.

Feingold, G., R. Furrer, P. Pilewskie, L. A. Remer, Q. Min, and H. Jonsson (2006), Aerosol indirect effect studies at Southern Great Plains during the May 2003 Intensive Operations Period, *J. Geophys. Res.*, *111*, D05S14, doi:10.1029/2004JD005648.

Ferrare, R. A., et al. (2004), Raman lidar measurements of aerosols and water vapor during the May 2003 Aerosol IOP, Fourteenth ARM Science Team Meeting Proceedings, Albuquerque, New Mexico. (Available at http://www.arm.gov/publications/proceedings/conf14/author.stm)

Ferrare, R., et al. (2006), Evaluation of daytime measurements of aerosols and water vapor made by an operational Raman lidar over the Southern Great Plains, *J. Geophys. Res.*, *111*, D05S08, doi:10.1029/2005JD005836.

Goldsmith, J. E. M., F. H. Blair, S. E. Bisson, and D. D. Turner (1998), Turnkey Raman lidar for profiling atmospheric water vapor, clouds, and aerosols, *Appl. Opt.*, *37*, 4979–4990.

Hänel, G. (1976), The properties of atmospheric aerosol particles as functions of the relative humidity at thermodynamic equilibrium with the surrounding moist air, *Adv. Geophys.*, *19*, 73–188.

Hansell, R. A., S.-C. Tsay, Q. Ji, N. C. Hsu, M.-J. Jeong, S. H. Wang, K. N. Liou, and S. C. Ou (2009), An assessment of surface longwave direct radiative effect of airborne saharan dust during the NAMMA field campaign, *J. Atmos. Sci.*, *67*(4), 1048–1065, doi:10.1175/2009JAS3257.1.

Hegg, D. A., L. F. Radke, and P. V. Hobbs (1990), Particle production associated with marine clouds, *J. Geophys. Res.*, *95*(D9), 13,917–13,926, doi:10.1029/JD095iD09p13917.

Hegg, D. A., D. S. Covert, M. J. Rood, and P. V. Hobbs (1996), Measurements of aerosol optical properties in marine air, *J. Geophys. Res.*, *101*(D8), 12,893–12,903, doi:10.1029/96JD00751.

Hegg, D. A., D. S. Covert, H. Jonsson, D. Khelif, and C. A. Friehe (2004), Observations of the impact of cloud processing on aerosol light-scattering efficiency, *Tellus, Ser B*, *56*, 285–293.

Holben, B. N., et al. (1998), AERONET—A federated instrument network and data archive for aerosol characterization, *Remote Sens. Environ.*, *66*, 1–16.

Hoppel, W. A., J. W. Fitzgerald, G. M. Frick, and R. E. Larson (1990), Aerosol size distributions and optical properties found in the marine boundary layer over the Atlantic Ocean, *J. Geophys. Res.*, *95*(D4), 3659–3686, doi:10.1029/JD095iD04p03659.

Hoppel, W. A., G. M. Frick, J. W. Fitzgerald, and R. E. Larson (1994), Marine boundary layer measurements of new particle formation and the effects nonprecipitating clouds have on aerosol size distribution, *J. Geophys. Res.*, *99*(D7), 14,443–14,459, doi:10.1029/94JD00797.

Ignatov, A., and N. R. Nalli (2002), Aerosol retrievals from multiyear multisatellite AVHR Pathfinder Atmosphere (PATMOS) data set for correcting remotely sensed sea surface temperatures, *J. Atmos. Oceanic Technol.*, *19*, 1986–2008.

Intergovernmental Panel on Climate Change (2007), *Climate Change 2007: The Physical Science Basis, Contribution of Working Group I to the Fourth Assessment Report of the Intergovernmental Panel on Climate Change*, edited by S. Solomon et al., 996 pp., Cambridge Univ. Press, Cambridge, UK.

Jeong, M.-J., and N. C. Hsu (2008), Retrievals of aerosol single-scattering albedo and effective aerosol layer height for biomass-burning smoke: Synergy derived from "A-Train" sensors, *Geophys. Res. Lett.*, *35*, L24801, doi:10.1029/2008GL036279.

Jeong, M.-J., and Z. Li (2005), Quality, compatibility and synergy analyses of global aerosol products derived from the advanced very high resolution radiometer and total ozone mapping spectrometer, *J. Geophys. Res.*, *110*, D10S08, doi:10.1029/2004JD004647.

Jeong, M.-J., Z. Li, D. A. Chu, and S.-C. Tsay (2005), Quality and compatibility analyses of global aerosol products derived from the advanced very high resolution radiometer and moderate resolution imaging spectroradiometer, *J. Geophys. Res.*, *110*, D10S09, doi:10.1029/2004JD004648.

Jeong, M.-J., Z. Li, E. Andrews, and S.-C. Tsay (2007), Effect of aerosol humidification on the column aerosol optical thickness over the Atmospheric Radiation Measurement Southern Great Plains site, *J. Geophys. Res.*, *112*, D10202, doi:10.1029/2006JD007176.

Kasten, F. (1969), Visibility in the phase of precondensation, *Tellus*, *21*, 631–635.

Kaufman, Y. J., et al. (2005), A critical examination of the residual cloud contamination and diurnal sampling effects on MODIS estimates of aerosol over ocean, *IEEE Trans. Geosci. Remote Sens.*, *43*(12), 2886–2897.

Kinne, S., T. P. Ackerman, M. Shiobara, A. Uchiyama, A. J. Heymsfield, L. Miloshevich, J. Wendell, E. W. Eloranta, C. Purgold, and R. W. Bergstrom (1997), Cirrus cloud radiative and microphysical properties from ground observations and in situ measurements during FIRE 1991 and their application to exhibit problems in cirrus solar radiative transfer modeling, *J. Atmos. Sci.*, *54*, 2320–2344, doi:10.1175/1520-0469(1997)054<2320:CCRAMP>2.0.CO;2.

Koren, I., Y. J. Kaufman, L. A. Remer, and J. V. Martins (2004), Measurement of the effect of Amazon smoke on inhibition of cloud formation, *Science*, *303*(5662), 1342–1345, doi:10.1126/science.1089424.

Koren, I., L. A. Remer, Y. J. Kaufman, Y. Rudich, and J. V. Martins (2007), On the twilight zone between clouds and aerosols, *Geophys. Res. Lett.*, *34*, L08805, doi:10.1029/2007GL029253.

Kotchenruther, R. A., P. V. Hobbs, and D. A. Hegg (1999), Humidification factors for atmospheric aerosols off the mid-Atlantic coast of the United States, *J. Geophys. Res.*, *104*(D2), 2239–2251, doi:10.1029/98JD01751.

Loeb, N. G., and G. L. Schuster (2008), An observational study of the relationship between cloud, aerosol and meteorology in broken low-level cloud conditions, *J. Geophys. Res.*, *113*, D14214, doi:10.1029/2007JD009763.

Long, C. N., D. W. Slater, and T. Toonman (2001), Total Sky Imager Model 880 status and testing results, *ARM TR-006*, 36 pp.

Marshak, A., G. Wen, J. A. Coakley Jr., L. A. Remer, N. G. Loeb, and R. F. Cahalan (2008), A simple model for the cloud adjacency effect and the apparent bluing of aerosols near clouds, *J. Geophys. Res.*, *113*, D14S17, doi:10.1029/2007JD009196.

Matheson, M. A., J. A. Coakley Jr., and W. R. Tahnk (2006), Multiyear advanced very high resolution radiometer observations of summertime stratocumulus collocated with aerosols in the northeastern Atlantic, *J. Geophys. Res.*, *111*, D15206, doi:10.1029/2005JD006890.

McComiskey, A., G. Feingold, A. S. Frisch, D. D. Turner, M. A. Miller, J. C. Chiu, Q. Min, and J. A. Ogren (2009), An assessment of aerosol-cloud interactions in marine stratus clouds based on surface remote sensing, *J. Geophys. Res.*, *114*, D09203, doi:10.1029/2008JD011006.

Öström, E., and K. J. Noone (2000), Vertical profiles of aerosol scattering and absorption measured in situ during North Atlantic Aerosol Characterization Experiments, *Tellus, Ser. B*, *52*, 526–545, doi:10.1034/j.1600-0889.2000.00050.x.

Rainwater, M., and L. Gregory (2005), Cimel Sun photometer (CSPHOT) handbook, 14 pp., *ARM TR-056*. (Available at http://www.arm.gov/instruments/)

Sheridan, P. J., A. Jefferson, and J. A. Ogren (2002), Spatial variability of submicrometer aerosol radiative properties over the Indian Ocean during INDOEX, *J. Geophys. Res.*, *107*(D19), 8011, doi:10.1029/2000JD000166.

Small, J. D., P. Y. Chuang, G. Feingold, and H. Jiang (2009), Can aerosol decrease cloud lifetime?, *Geophys. Res. Lett.*, *36*, L16806, doi:10.1029/2009GL038888.

Smirnov, A., B. N. Holben, T. F. Eck, O. Dubovik, and I. Slutsker (2000), Cloud-screening and quality control algorithms for the AERONET database, *Remote Sens. Environ.*, *73*, 337–349.

Su, W., G. L. Schuster, N. G. Loeb, R. R. Rogers, R. A. Ferrare, C. A. Hostetler, J. W. Hair, and M. D. Obland (2008), Aerosol and cloud interaction observed from high spectral resolution lidar data, *J. Geophys. Res.*, *113*, D24202, doi:10.1029/2008JD010588.

Tackett, J. L., and L. Di Girolamo (2009), Enhanced aerosol backscatter adjacent to tropical trade wind clouds revealed by satellite-based lidar, *Geophys. Res. Lett.*, *36*, L14804, doi:10.1029/2009GL039264.

Twohy, C. H., J. A. Coakley Jr., and W. R. Tahnk (2009), Effect of changes in relative humidity on aerosol scattering near clouds, *J. Geophys. Res.*, *114*, D05205, doi:10.1029/2008JD010991.

Turner, D. D. (2004), Raman lidar (RL) handbook, *ARM TR-038*, 13 pp. (Available at http://www.arm.gov/instruments/)

Turner, D. D., and J. E. M. Goldsmith (1999), Twenty-four hour Raman lidar measurements during the Atmospheric Radiation Measurement program's 1996 and 1997 water vapor intensive observation periods, *J. Atmos. Oceanic Technol.*, *16*, 1062–1076.

Turner, D. D., R. A. Ferrare, L. A. H. Brasseur, W. F. Feltz, and T. P. Toonman (2002), Automated retrievals of water vapor and aerosol profiles from an operational Raman lidar, *J. Atmos. Oceanic Technol.*, *19*, 37–50.

Wen, G., A. Marshak, R. F. Cahalan, L. A. Remer, and R. G. Kleidman (2007), 3D aerosol-cloud radiative interaction observed in collocated MODIS and ASTER images of cumulus cloud fields, *J. Geophys. Res.*, *112*, D13204, doi:10.1029/2006JD008267.

Yuan, T., Z. Li, R. Zhang, and J. Fan (2008), Increase of cloud droplet size with aerosol optical depth: An observation and modeling study, *J. Geophys. Res.*, *113*, D04201, doi:10.1029/2007JD008632.

Zhang, J., J. S. Reid, and B. N. Holben (2005), An analysis of potential cloud artifacts in MODIS over ocean aerosol optical thickness products, *Geophys. Res. Lett.*, *32*, L15803, doi:10.1029/2005GL023254.

M.-J. Jeong, NASA Goddard Space Flight Center, Code 613.2, Greenbelt, MD 20771, USA. (myeong-jae.jeong@nasa.gov)

Z. Li, Department of Atmospheric and Oceanic Science, University of Maryland, College Park, MD 20742, USA.